J|A|C|S
ARTICLES
Published on Web 08/08/2006

Directed Assembly of Mesoscopic Metallocycles with Controllable Size, Chirality, and Functionality Based on the Robust Pt−Alkynyl Linkage

Hua Jiang and Wenbin Lin*

Contribution from the Department of Chemistry, CB#3290, University of North Carolina, Chapel Hill, North Carolina 27599

Received May 11, 2006; E-mail: wlin@unc.edu

Abstract: This paper describes expeditious stepwise directed assembly of large homochiral metallocycles with up to 38 6,6′-bis(alkynyl)-1,1′-binaphthalene bridging ligands (**L**) and 38 *trans*-Pt(PEt_3)$_2$ ([**Pt**]) centers and with cavities as large as 22 nm in diameter. These unprecedented mesoscopic metallocycles are synthesized by cyclization of different lengths of oligomeric building blocks, $\mathbf{L}_m[\mathbf{Pt}]_{m+1}Cl_2$ ($m = 1$, 2, 3, 5, 7, 11, 19, and 31) and $[\mathbf{Pt}]_n\mathbf{L}_{n+1}H_2$ ($n = 1$, 2, 3, 4, 5, 6, 10, 18, and 30), and have been characterized by a variety of techniques, including $^1H\{^{31}P\}$, $^{13}C\{^1H\}$, and $^{31}P\{^1H\}$ NMR spectroscopy, MALDI-TOF MS, elemental analysis, FT-IR, UV−vis, CD, size-exclusion chromatography, and diffusion-ordered NMR spectroscopy. The present synthetic methodology was also extended to the synthesis of non-homochiral metallocycles of very different topologies and macrocyclic structures with additional functional groups precisely placed at different positions. This work provides a general strategy for the construction of nanoscopic and mesoscopic functional supramolecular architectures of controllable size, chirality, and functionality that cannot be accessed from the existing synthetic approaches.

1. Introduction

One of the most important goals of contemporary chemistry is to mimic the form and function of Nature's highly efficient biochemical machineries, but this dream cannot be realized before the development of efficient synthetic methodologies that allow rapid assembly of large and complex systems in a programmed fashion.[1] To this end, synthetic chemists have strived to construct supramolecular architectures starting from well-defined building blocks via self-assembly processes.[2] The past few decades have witnessed tremendous progress in this research area, and many aesthetically appealing or/and functional supramolecular systems have been rationally assembled.[2,3]

Of all the supramolecular systems, macrocyclic compounds are among the most widely studied.[4] The introduction of noncovalent bonds, such as metal−ligand coordination bonds, has overcome the typically low yield for the stepwise synthesis of macrocycles based on covalent bonds. As first formulated by Fujita et al. and Stang et al.,[2] nanoscopic metallocycles are typically assembled from appropriate well-defined rigid and directional building blocks, which can be classified into two types: linear and angular subunits. Each subunit has two active functional end groups to interact with the other building block. By using appropriate angular and linear building blocks, numerous small-molecular polygons have been assembled. Most of known metallocycles are of small size, such as triangles and squares.[3,5] Larger polygonal structures have been, however, more scarce prior to our work, as a direct consequence of their entropic disadvantage. While a few molecular hexagons are known,[6] there are far fewer examples of molecular pentagons,[7] heptagons,[8] and octagons.[9]

We have recently become interested in the construction of functional chiral metallocycles by using rigid atropisomeric bridging ligands and appropriate metal connectors as the

(1) Lehn, J.-M. *Supramolecular Chemistry: Concepts and Perspectives*; VCH Publishers: New York, 1995.
(2) (a) Fujita, M.; Ogura, K. *Coord. Chem. Rev.* **1996**, *148*, 249. (b) Fujita, M. *Chem. Soc. Rev.* **1998**, *27*, 417. (c) Stang, P. J.; Olenyuk, B. *Acc. Chem. Res.* **1997**, *30*, 502. (d) Seidel, S. R.; Stang, P. J. *Acc. Chem. Res.* **2002**, *35*, 972.
(3) (a) Holliday, B. J.; Mirkin, C. A. *Angew. Chem., Int. Ed.* **2001**, *40*, 2022. (b) Gianneschi, N. C.; Masar, M. S., III; Mirkin, C. A. *Acc. Chem. Res.* **2005**, *38*, 825. (c) Li, D.; Parkin, S.; Wang, G.; Yee, G. T.; Clerac, R.; Wernsdorfer, W.; Holmes, S. M. *J. Am. Chem. Soc.* **2006**, *128*, 4214. (d) Kuhlman, M. L.; Rauchfuss, T. B. *J. Am. Chem. Soc.* **2003**, *125*, 10084. (e) Lau, V. C.; Berben, L. A.; Long, J. R. *J. Am. Chem. Soc.* **2002**, *124*, 9042. (f) Wilson, J. N.; Bunz, U. H. F. *J. Am. Chem. Soc.* **2005**, *127*, 4124. (g) Wang, W.; Wan, W.; Zhou, H. H.; Niu, S. Q.; Li, A. D. Q. *J. Am. Chem. Soc.* **2003**, *125*, 5248. (h) Caulder, D. L.; Raymond, K. N. *J. Chem. Soc., Dalton Trans.* **1999**, 1185.
(4) Helgeson, R. C.; Weisman, G. R.; Toner, J. L.; Tarnowski, T. L.; Chao, Y.; Mayer, J. M.; Cram, D. J. *J. Am. Chem. Soc.* **1979**, *101*, 4928.
(5) (a) Leininger, S.; Olenyuk, B.; Stang, P. J. *Chem. Rev.* **2000**, *100*, 853. (b) Onitsuka, K.; Yamamoto, S.; Takahashi, S. *Angew. Chem., Int. Ed.* **1999**, *38*, 174.
(6) (a) Stang, P. J.; Persky, N. E.; Manna, J. *J. Am. Chem. Soc.* **1997**, *119*, 4777. (b) Saalfrank, R. W.; Bernt, I.; Uller, E.; Hampel, F. *Angew. Chem., Int. Ed. Engl.* **1997**, *36*, 2482. (c) Newkome, G. R.; Cho, T. J.; Moorefield, C. N.; Baker, G. R.; Cush, R.; Russo, P. S. *Angew. Chem., Int. Ed.* **1999**, *38*, 3717. (d) Matsumoto, N.; Motoda, Y.; Matsuo, T.; Nakashima, T.; Re, N.; Dahan, F.; Tuchagues, J. P. *Inorg. Chem.* **1999**, *38*, 1165. (e) Mamula, O.; von Zelewsky, A.; Bernardinelli, G. *Angew. Chem., Int. Ed.* **1998**, *37*, 290. (f) Lai, S. W.; Cheung, K. K.; Chan, M. C. W.; Che, C. M. *Angew. Chem., Int. Ed.* **1998**, *37*, 182.
(7) Hasenknopf, B.; Lehn, J. M.; Boumediene, N.; DupontGervais, A.; VanDorsselaer, A.; Kneisel, B.; Fenske, D. *J. Am. Chem. Soc.* **1997**, *119*, 10956.
(8) Ali, M. M.; MacDonnell, F. M. *J. Am. Chem. Soc.* **2000**, *122*, 11527.
(9) Jones, P. L.; Byrom, K. J.; Jeffery, J. C.; McCleverty, J. A.; Ward, M. D. *Chem. Commun.* **1997**, 1361.

10.1021/ja0633013 CCC: $33.50

Scheme 1

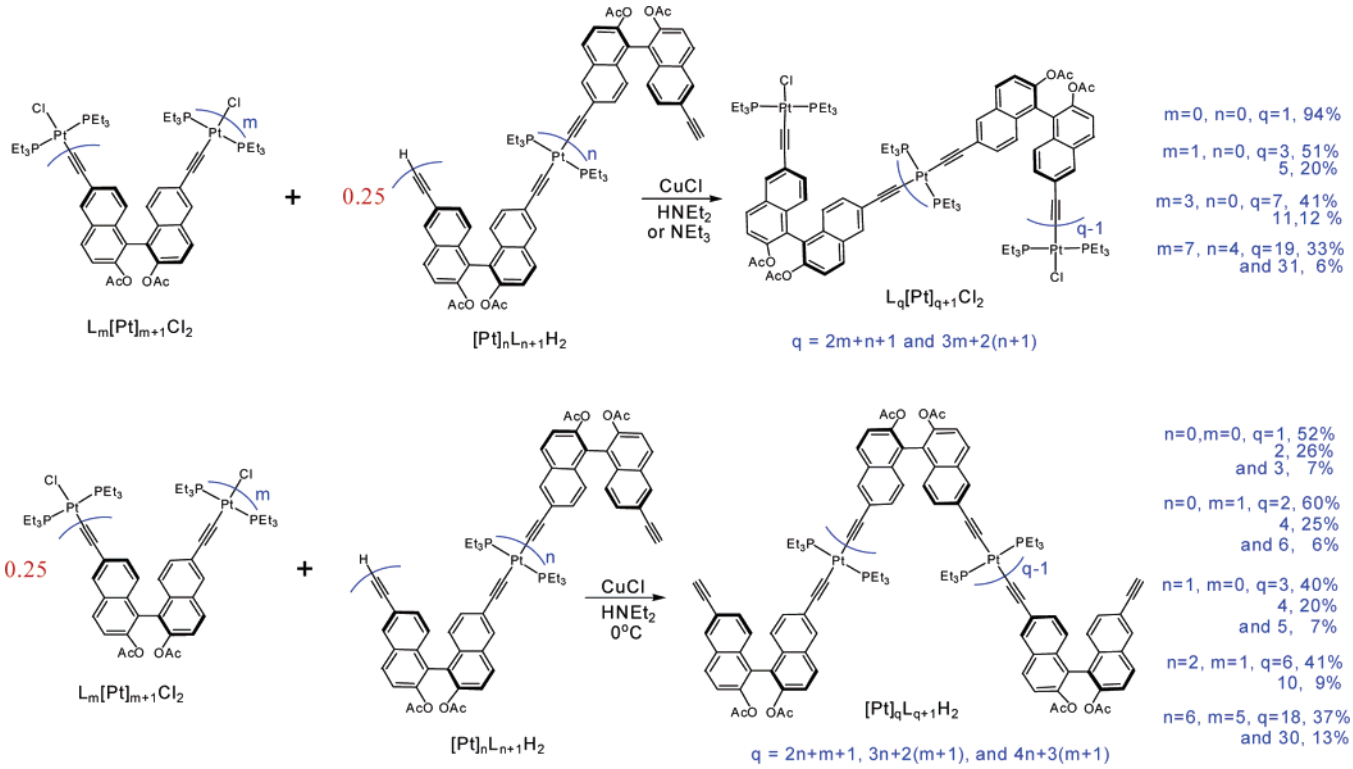

building blocks, with the hope of generating well-defined enzyme-like chiral pockets or functionalities. By taking advantage of the kinetic inertness of the robust Pt−alkynyl linkage, we have achieved the self-assembly of chiral dimeric metallocyclophanes,[10] triangles,[11] and squares[12] by using *cis*-Pt(PEt_3)$_2$ as an angular metal corner. We have also described efficient one-pot self-assembly of chiral metallocycles ranging from triangles to octagons by using *trans*-Pt(PEt_3)$_2$ as a linear metal linker.[13] This method is, however, not amenable to the synthesis of even larger molecular polygons because of their very low synthetic efficiency and the difficulty of separating very large polygons from each other. Herein we report the expeditious stepwise directed assembly of large chiral metallocycles with up to 38 bridging ligands (**L**) and 38 *trans*-Pt(PEt_3)$_2$ (**[Pt]**) centers and with cavities as large as 22 nm in diameter. These unprecedented mesoscopic metallocycles were synthesized by cyclization of different lengths of oligomeric building blocks, $\mathbf{L}_m[\mathbf{Pt}]_{m+1}Cl_2$ (m = 1, 2, 3, 5, 7, 11, 19, and 31) and $[\mathbf{Pt}]_n\mathbf{L}_{n+1}H_2$ (n = 1, 2, 3, 4, 5, 6, 10, 18, and 30), and have been characterized by a variety of different techniques, including $^1H\{^{31}P\}$, $^{13}C\{^1H\}$, and $^{31}P\{^1H\}$ NMR spectroscopy, MALDI-TOF MS, elemental analysis, FT-IR, UV−vis, CD, size-exclusion chromatography, and diffusion-ordered NMR spectroscopy (DOSY). A preliminary account on the directed assembly of chiral metallocycles that are isomeric to the present systems was previously reported.[14]

(10) (a) Hua, J.; Lin, W. *Org. Lett.* **2004**, *6*, 861. (b) Jiang, H.; Hu, A. G.; Lin, W. *Chem. Commun.* **2003**, 96.
(11) Lee, S. J.; Hu, A. G.; Lin, W. *J. Am. Chem. Soc.* **2002**, *124*, 12948.
(12) Lee, S. J.; Luman, C. R.; Castellano, F. N.; Lin, W. B. *Chem. Commun.* **2003**, 2124.
(13) (a) Jiang, H.; Lin, W. *J. Am. Chem. Soc.* **2003**, *125*, 8084. (b) Jiang, H.; Lin, W. *J. Organomet. Chem.* **2005**, *690*, 5159.
(14) Jiang, H.; Lin, W. *J. Am. Chem. Soc.* **2004**, *126*, 7426.

2. Experimental Section

Materials. All of the ligands are chiral, and the resulting oligomers and metallocycles are homochiral and can be either the (*S*)- or (*R*)-enantiomer unless specified otherwise. All of the chemicals were obtained from commercial sources and used without further purification. All of the reactions and manipulations were carried out under N_2 with the use of standard inert atmosphere and Schlenk techniques. Solvents used in reactions were dried by standard procedures. The IR spectra were recorded from KBr pellets on a Nicolet Magna-560 FT-IR spectrometer. NMR spectra were recorded on a Bruker NMR 400 DRX spectrometer. ^1H NMR spectra were recorded at 400 MHz and referenced to the proton resonance resulting from incomplete deuteration of chloroform (δ 7.26). $^{13}C\{^1H\}$ NMR spectra were recorded at 100 MHz, and all of the chemical shifts are reported downfield in ppm relative to the carbon resonance of chloroform-d_1 (δ 77.0). The synthesis of 2,2′-diacetoxy-6,6′-diethynyl-1,1′-binaphthalene (**L**-H_2) was reported in our previous work.[10b] All of the spectroscopic and other characterization data are included in the Supporting Information.

General Procedures for the Synthesis of Homochiral $\mathbf{L}_m$-$[\mathbf{Pt}]_{m+1}\mathbf{Cl}_2$. To a solution of $[\mathbf{Pt}]_n\mathbf{L}_{n+1}H_2$ and an excess amount of $\mathbf{L}_m$-$[\mathbf{Pt}]_{m+1}Cl_2$ in deareated CH_2Cl_2 and NEt_3 was added a catalytic amount of CuCl. After stirring at room temperature for typically 40 min, the reaction mixture was washed with water three times. The organic layer was dried over anhydrous $MgSO_4$, and the organic volatiles were removed in vacuo. The residue was purified by silica gel column flash chromatography to afford $\mathbf{L}_{2m+n+1}[\mathbf{Pt}]_{2m+n+2}Cl_2$, $\mathbf{L}_{3m+2n+2}[\mathbf{Pt}]_{3m+2n+3}Cl_2$, and $\mathbf{L}_{4m+3n+3}[\mathbf{Pt}]_{4m+3n+4}Cl_2$ as light yellow solids. The metal-terminated oligomers with an ethyl protecting group (**L**-OEt) were prepared similarly. Detailed synthetic procedures can be found in the Supporting Information, while the yields for homochiral metal-terminated oligomers with ligands **L** are listed in Scheme 1.

General Procedures for the Synthesis of Homochiral $[\mathbf{Pt}]_n\mathbf{L}_{n+1}\mathbf{H}_2$. To a solution of $\mathbf{L}_m[\mathbf{Pt}]_{m+1}Cl_2$ and an excess amount of $[\mathbf{Pt}]_n\mathbf{L}_{n+1}H_2$ in deareated CH_2Cl_2 and NEt_3 was added a catalytic amount of CuCl. After stirring at 0 °C for typically 40 min, the reaction mixture was quickly filtered through silica gel. After removal of the volatile organic

solvents in vacuo, the residue was purified by silica gel column flash chromatography to afford $[\mathbf{Pt}]_{2n+m+1}\mathbf{L}_{2n+m+2}H_2$, $[\mathbf{Pt}]_{3n+2m+2}\mathbf{L}_{3n+2m+3}H_2$, and $[\mathbf{Pt}]_{4n+3m+3}\mathbf{L}_{4n+3m+4}H_2$ as light yellow solids. The alkyne-terminated oligomers with an ethyl protecting group (**L**-OEt) were prepared similarly. Detailed synthetic procedures can be found in the Supporting Information, while the yields for homochiral ligand-terminated oligomers with ligands **L** are listed in Scheme 1.

Synthesis of (*RSR*)-$[\mathbf{Pt}]_2\mathbf{L}_3H_2$ and (*RSRSR*)-$[\mathbf{Pt}]_4\mathbf{L}_5H_2$. A mixture of (*S*)-**L**$[\mathbf{Pt}]_2Cl_2$ (280 mg, 0.207 mmol), (*R*)-**L**-H_2 (347 mg, 0.829 mmol), CH_2Cl_2 (5 mL), NEt_3 (0.2 mL), and CuCl (10 mg, 0.1 mmol) was stirred at 0 °C for 40 min. The products were purified by silica gel column chromatography with dichloromethane/ethyl acetate (from 30:1 to 15:1, v/v). Yield: (*RSR*)-$[\mathbf{Pt}]_2\mathbf{L}_3H_2$, 270 g, 62%; (*RSRSR*)-$[\mathbf{Pt}]_4\mathbf{L}_5H_2$, 78 mg, 20%.

General Procedure for the Synthesis of Homochiral Metallocycles. To a solution of $\mathbf{L}_m[\mathbf{Pt}]_{m+1}Cl_2$ and $[\mathbf{Pt}]_n\mathbf{L}_{n+1}$-$H_2$ (1:1 molar ratio) in deareated CH_2Cl_2 and NEt_3 was added a catalytic amount of CuCl. After stirring at room temperature for typically ~18 h, the reaction mixture was washed with water three times. The organic layer was dried over anhydrous $MgSO_4$, and the organic volatiles were removed in vacuo. The residue was purified by silica gel column flash chromatography to afford [*trans*-$(PEt_3)_2Pt\mathbf{L}]_{m+n+1}$, [*trans*-$(PEt_3)_2Pt\mathbf{L}]_{2(m+n+1)}$, and [*trans*-$(PEt_3)_2Pt\mathbf{L}]_{3(m+n+1)}$ as light yellow solids. Homochiral metallocycles [*trans*-$(PEt_3)_2Pt$(**L**-OEt)$]_n$ ($n = 3$ or 4) were synthesized similarly. The details can be found in the Supporting Information, while yields for all of the homochiral metallocycles with ligands **L** are listed in Table 1.

Synthesis of (*RRRS*)-[*trans*-$(PEt_3)_2Pt\mathbf{L}]_4$ and (*RRRSRRRS*)-[*trans*-$(PEt_3)_2Pt\mathbf{L}]_8$. A mixture of (*S*)-**L**$[\mathbf{Pt}]_2Cl_2$ (54.2 mg, 0.0256 mmol), (*RRR*)-$[\mathbf{Pt}]_2\mathbf{L}_3H_2$ (34.5 mg, 0.0256 mmol), CH_2Cl_2 (300 mL), NEt_3 (1 mL), and CuCl (2 mg, 0.02 mmol) was stirred at room temperature for 18 h. The products were purified by silica gel column chromatography with dichloromethane/ethyl acetate (from 18:1 to 12:1, v/v). Yield: (*RRRS*)-[*trans*-$(PEt_3)_2Pt\mathbf{L}]_4$, 73 mg, 83%; (*RRRSRRRS*)-[*trans*-$(PEt_3)_2Pt\mathbf{L}]_8$, 9 mg, 10%.

Synthesis of (*RRSS*)-[*trans*-$(PEt_3)_2Pt\mathbf{L}]_4$ and (*RRSSRRSS*)-[*trans*-$(PEt_3)_2Pt\mathbf{L}]_8$. A mixture of (*RR*)-$\mathbf{L}_2[\mathbf{Pt}]_3Cl_2$ (54.9 mg, 0.025 mmol), (*SS*)-$[\mathbf{Pt}]$(**L**-H)$_2$ (31.6 mg, 0.025 mmol), CH_2Cl_2 (300 mL), NEt_3 (1 mL), and CuCl (2 mg, 0.02 mmol) was stirred at room temperature for 18 h. The products were purified by silica gel column chromatography with dichloromethane/ethyl acetate (from 18:1 to 12:1, v/v). Yield: (*RRSS*)-[*trans*-$(PEt_3)_2Pt\mathbf{L}]_4$, 65 mg, 76%; (*RRSSRRSS*)-[*trans*-$(PEt_3)_2Pt\mathbf{L}]_8$, 10 mg, 12%.

Synthesis of (*RSRS*)-[*trans*-$(PEt_3)_2Pt\mathbf{L}]_4$ and (*RSRSRSRS*)-[*trans*-$(PEt_3)_2Pt\mathbf{L}]_8$. A mixture of (*S*)-**L**$[\mathbf{Pt}]_2Cl_2$ (37.4 mg, 0.0277 mmol), (*RSR*)-$[\mathbf{Pt}]_2\mathbf{L}_3H_2$ (58.6 mg, 0.0277 mmol), CH_2Cl_2 (300 mL), NEt_3 (1 mL), and CuCl (2 mg, 0.02 mmol) was stirred at room temperature for 18 h. The products were purified by silica gel column chromatography with dichloromethane/ethyl acetate (from 18:1 to 12:1, v/v). Yield: (*RSRS*)-[*trans*-$(PEt_3)_2Pt\mathbf{L}]_4$, 71 mg, 76%; (*RSRSRSRS*)-[*trans*-$(PEt_3)_2Pt\mathbf{L}]_8$, 7 mg, 8%.

Synthesis of (*RSRS*)-[*trans*-$(PEt_3)_2Pt$(L**-OEt)$]_4$.** A mixture of (*S*)-(**L**-OEt)$[\mathbf{Pt}]_2Cl_2$ (21.2 mg, 0.016 mmol), (*R*)-**L**-OEt-H_2 (6.5 mg, 0.016 mmol), $HNEt_2$ (12 mL), and CuCl (1 mg, 0.01 mmol) was stirred at room temperature for 18 h. The product was purified by silica gel column chromatography with hexane/dichloromethane/ethyl acetate (6:1:1, v/v/v). Yield: (*RSRS*)-[*trans*-$(PEt_3)_2Pt$(**L**-OEt)$]_4$, 6 mg, 23%.

Synthesis of Homochiral Metallocycles [*trans*-$(PEt_3)_2Pt]_4\mathbf{L}_3$(L**-OEt) and {[*trans*-$(PEt_3)_2Pt]_4\mathbf{L}_3$(**L**-OEt)}$_2$.** A mixture of $\mathbf{L}_3[\mathbf{Pt}]_4Cl_2$ (98.8 mg, 0.0325 mmol), **L**-OEt-H_2 (13.2 mg, 0.0325 mmol), CH_2Cl_2 (300 mL), NEt_3 (1 mL), and CuCl (2 mg, 0.02 mmol) was stirred at room temperature for 18 h. The products were purified by silica gel column chromatography with dichloromethane/ethyl acetate (from 18:1 to 15:1, v/v). Yield: [*trans*-$(PEt_3)_2Pt]_4\mathbf{L}_3$(**L**-OEt), 90 mg, 83%; {[*trans*-$(PEt_3)_2Pt]_4\mathbf{L}_3$(**L**-OEt)}$_2$, 14 mg, 13%.

MALDI-TOF MS was carried out on a Voyager-DE PRO instrument at Duke University. 2,5-Dihydroxybenzoic acid was used as the matrix for shorter open oligomers ($m = 1, 2, 3, 5, 7$ and $n = 1, 2, 3, 4, 5, 6$), and the peaks were calibrated using insulin in the linear model. 1,8,9-Trihydroxyanthracene was used as the matrix for longer open oligomers ($m = 19$ and $n = 18$) and larger metallocycles (9mer to 22 mer), and the peaks were calibrated using myoglobin in the linear model.

Optical Measurements (UV−Vis and CD). UV−visible spectra were obtained using a Shimadzu UV-2410PC spectrophotometer. Circular dichroism (CD) spectra were recorded on a Jasco J-720 spectropolarimeter. Oligomers and cycles were dissolved in acetonitrile with concentrations on the order of 10^{-6}−10^{-5} M. Due to the poor solubility of longer oligomers and larger metallocycles in acetonitrile, they were dissolved in acetonitrile with the addition of varying amounts of dichloromethane. The measurements were carried out in 1 mm cells. Smaller oligomers $\mathbf{L}_m[\mathbf{Pt}]_{m+1}Cl_2$ ($m = 1, 2, 3$, and 5) and $[\mathbf{Pt}]_n\mathbf{L}_{n+1}H_2$ ($n = 1, 2, 3$, and 4) were dissolved in acetonitrile. $\mathbf{L}_7[\mathbf{Pt}]_8Cl_2$ and $[\mathbf{Pt}]_5\mathbf{L}_6H_2$ were dissolved in acetonitrile with 0.8% dichloromethane. Longer oligomers $\mathbf{L}_m[\mathbf{Pt}]_{m+1}Cl_2$ ($m = 11, 19$, and 31), $[\mathbf{Pt}]_n\mathbf{L}_{n+1}H_2$ ($n = 6, 10, 18$, and 30), and metallocycles from 9mer to 38mer were dissolved in dichloromethane.

Size-Exclusion Chromatography (SEC). SEC was performed on an HPLC using PLgel columns (Polymer Laboratories, 5 μm, 7.5 × 300 mm) of 10^3 Å pore size. Conditions: mobile phase, dichloromethane (Aldrich, Certified A.C.S.); flow rate, 0.25 mL/min; injection volume, 10 μL. Sample detection was achieved by absorption spectroscopy using a diode array detector at 300 nm (±10 nm bandwidth). Polystyrene standards (MW = 2500, 13000, 30000, and 50000) were purchased from Aldrich. Polystyrene was detected at a wavelength of 254 nm.

Diffusion Ordered NMR Spectroscopy (DOSY). DOSY spectra were taken on a Varian INOVA 600 equipped with a 20 A gradient driver. Samples were prepared in $CDCl_3$ with the concentration of 8.3 mg/mL. A 5 mm Nalorac H−F diffusion probe was used with dry N_2; room-temperature gas provides cooling for the probe's gradient coils. The sample was maintained at 25 ± 0.5 °C and checked with an ethylene glycol or methanol sample. Acquisition parameters were optimized using a standard 1D ^{1}H experiment and the BPPSTE or BPPLED pulse sequence with the minimum gradient level.[15] Metallocycles of $q = 3, 4, 5, 6, 7, 8, 10, 12, 14$, and 22 were run with the BPPSTE sequence. Metallocycles of $q = 22$ and 38 were run with the BPPLED sequence. Typically 8K points were acquired in 700 ms, covering a spectrum width of 6K Hz. At a transmitter power of 59 dB, the 90° pulse width was 6.5 s, and the receiver gain was set to 30−40. Relaxation times T_1 were determined using the inversion recovery and CPMG pulse sequences, respectively. For the diffusion experiments, the relaxation delay was set to 1−2 T_1. The maximum gradient level was selected to yield peak intensities at ~10% of the peak intensity at the minimum gradient level. An array of 12 gradient values was used, with the squares of the gradient strengths varying linearly between the minimum (~7 G/cm) and the maximum (70−100 G/cm). For each gradient level, 32−256 steady-state pulses and 64−256 transients were used. Typical values were 64 steady-state runs and 64 transients per gradient level. A relaxation delay time of 6 s was optimal, and a diffusion time of 50 ms was used in all diffusion experiments. Square, 1 ms gradient pulses were used with a gradient delay time of 0.3 ms. A longitudinal eddy delay time of 10 ms was used in the BPPLED experiments.

3. Results

3.1. Synthesis of Oligomeric Building Blocks. The requisite metal-terminated oligomers, $\mathbf{L}_m[\mathbf{Pt}]_{m+1}Cl_2$, and ligand-termi-

(15) (a) Wu, D.; Chen, A.; Johnson, C. S. *J. Magn. Reson. A* **1995**, *115*, 260. (b) Pelta, M. D.; Barjat, H.; Morris, G. A.; Davis, A. L.; Hammond, S. J. *Magn. Reson. Chem.* **1998**, *36*, 706.

nated oligomers, $[\mathbf{Pt}]_n\mathbf{L}_{n+1}H_2$, were synthesized via an iterative process, as shown in Scheme 1.[16] Treatment of **L**-H_2 with 2 equiv of *trans*-$Pt(PEt_3)_2Cl_2$ in the presence of a catalytic amount of CuCl in benzene and NEt_3 under reflux afforded $\mathbf{L}[\mathbf{Pt}]_2Cl_2$ in 91% yield. The longer metal-terminated oligomers, $\mathbf{L}_m[\mathbf{Pt}]_{m+1}Cl_2$ ($m = 1$, 2, 3, 5, 7, 11, 19, and 31), were prepared by treating excess amounts of shorter lengths of metal-terminated oligomers with 0.25 equiv of ligand-terminated oligomers $[\mathbf{Pt}]_n\mathbf{L}_{n+1}H_2$ at room temperature for ~40 min in deareated CH_2Cl_2 and NEt_3 in the presence of a catalytic amount of CuCl. For example, by treating $\mathbf{L}[\mathbf{Pt}]_2Cl_2$ with 0.25 equiv of **L**-H_2 at room temperature, two longer metal-terminated oligomers, $\mathbf{L}_3[\mathbf{Pt}]_4Cl_2$ (51%) and $\mathbf{L}_5[\mathbf{Pt}]_6Cl_2$ (20%), were obtained in 71% overall yield by column chromatography. Reaction of $\mathbf{L}_7[\mathbf{Pt}]_8Cl_2$ and 0.25 equiv of $[\mathbf{Pt}]_6\mathbf{L}_7H_2$ at room temperature led to even longer oligomers, $\mathbf{L}_{19}[\mathbf{Pt}]_{20}Cl_2$ (33%) and $\mathbf{L}_{31}[\mathbf{Pt}]_{32}Cl_2$ (6%).

Ligand-terminated oligomers $[\mathbf{Pt}]_n\mathbf{L}_{n+1}H_2$ ($n = 1$, 2, 3, 4, 5, 6, 10, 18, and 30) were similarly obtained by using excess **L**-H_2 in the iterative assembly processes. The ligand-terminated oligomers $[\mathbf{Pt}]_n\mathbf{L}_{n+1}H_2$ are not stable in these concentrations at room temperature and slowly reassemble to different lengths of oligomers in the presence of CuCl catalyst. This is probably because the acetylenic protons at the two ends of the oligomers can be activated by the Cu(I) species to attack the [**Pt**] centers to initiate reassembly reactions. In contrast, the lack of acetylenic protons in the preparation of metal-terminated oligomers leads to stable oligomers. Fortunately, this reassembly process of ligand-terminated oligomers does not occur at an appreciable rate at 0 °C. Thus, the syntheses of all ligand-terminated oligomers were carried out at 0 °C. $[\mathbf{Pt}]_{18}\mathbf{L}_{19}H_2$ and $[\mathbf{Pt}]_{30}\mathbf{L}_{31}H_2$, for example, were prepared by treating $\mathbf{[Pt]}_6\mathbf{L}_7H_2$ with 0.25 equiv of $\mathbf{L}_5\mathbf{[Pt]}_6Cl_2$ at 0 °C in yields of 37% and 13%, respectively.

In each of the above reactions, two or three major open oligomers of different lengths were isolated in high overall yields by silica gel column chromatography. It is important to note that, although only 2 equiv of $\mathbf{L}_m[\mathbf{Pt}]_{m+1}Cl_2$ or $[\mathbf{Pt}]_n\mathbf{L}_{n+1}H_2$ is needed stoichiometrically for the synthesis of longer oligomers, 4 equiv was employed in order to minimize the chance of forming cyclic species. Excess amounts of starting materials were recovered, and no cyclic species were observed in these reactions. The yields were thus calculated on the basis of the limiting starting materials.

3.2. Synthesis of Metallocycles. Under dilute conditions, treatment of metal-terminated $\mathbf{L}_m[\mathbf{Pt}]_{m+1}Cl_2$ with 1 equiv of ligand-terminated $[\mathbf{Pt}]_n\mathbf{L}_{n+1}H_2$ in the presence of a catalytic amount of CuCl in CH_2Cl_2 and $HNEt_2$ at room temperature afforded cyclic species in high overall yields (Scheme 2 and Table 1). For example, by treating equimolar $\mathbf{L}[\mathbf{Pt}]_2Cl_2$ and [**Pt**]-$\mathbf{L}_2H_2$, molecular triangle (37%), hexagon (36%), and nonagon (11%) were efficiently assembled (with an overall yield of 84%). Metallocycles of much larger sizes have been synthesized via this directed-assembly process. The chiral metallocycles of varying sizes resulted from [1+1], [2+2], and [3+3] cyclization processes, respectively. The reactions gave the highest yield for [1+1] product, followed by [2+2] and [3+3] products, for most reactions, with the exception of the syntheses of 3mer, 6mer, and 9mer, in which similar yields of [1+1] and [2+2] products were obtained, presumably due to the strain experienced by the trimer. In the synthesis of larger metallocycles, the efficiency of [3+3] cyclization products became very low, and the [3+3] products were not isolated. The efficiency of [2+2] cyclization is also low during the synthesis of even larger metallocycles. Only the [1+1] products were in fact isolated during the synthesis of 22mer and 38mer. As the sizes increase, the total yields of larger metallocycles decrease gradually, from a total yield of 97% for 4mer, 8mer, and 12mer to 25% for 38mer. All the metallocycles are stable under reaction conditions and were purified by silica gel column chromatography.

The largest metallocycle we have successfully synthesized contains 38 [**Pt**] and 38 **L** units, with a molecular mass of 32217.16 Da, and possesses an inner cavity of ~22 nm in diameter. The synthesis of 62mer by using oligomeric building blocks $\mathbf{L}_{31}[\mathbf{Pt}]_{32}Cl_2$ and $[\mathbf{Pt}]_{30}\mathbf{L}_{31}H_2$ failed, probably due to the greater distance between the ends of the "fused" open oligomer. When the rate for cyclization significantly slows, owing to the larger separation between the two ends, oligomerization will dominate and lead to intractable longer open oligomers. Molecular mechanics simulations indicated that the internal cavities of these molecular polygons range from 1.4 to 22 nm in diameter (Scheme 2).

These open metal- and ligand-terminated oligomers and metallocycles have been characterized by $^1H\{^{31}P\}$, $^{13}C\{^1H\}$, and $^{31}P\{^1H\}$ NMR spectroscopy, microanalysis, FT-IR, UV−vis, circular dichroism (CD), size-exclusion chromatography (SEC), and diffusion-ordered spectroscopy (DOSY). Most of the open oligomers (up to $m = 19$ and $n = 18$) and metallocycles (up to 22mer) have been characterized by MALDI-TOF MS.

3.3. Diagnostic NMR Spectroscopic Signals for Oligomers and Metallocycles. Metal-Terminated Open Oligomers $\mathbf{L}_m[\mathbf{Pt}]_{m+1}Cl_2$. The $^1H\{^{31}P\}$ NMR spectra are well separated into three groups: the signals between 7.9 and 7.1 ppm are assigned to the naphthyl groups, the signals between 2.3 and 2.0 and at ~1.2 ppm are assigned to the PEt_3 groups, and the singlet at ~1.88 ppm is assigned to the acetyl groups (Figure 1). Due to similar chemical environments of ligands **L** in oligomers, most of their $^1H\{^{31}P\}$ NMR peaks in the aromatic region overlap. Fortunately, the ratio between the two singlets at ~7.77 and ~7.74 ppm, which are assigned to the H5 and H5′ protons on the naphthalenes connecting to the terminal and inner [Pt] centers, respectively, provides a diagnostic for the length of the metal-terminated oligomers. As the chain length increases, the ratio decreases because the percentage of H5 decreases in the oligomers. The two sets of peaks at ~2.20 ($-PCH_2-$) and ~2.07 ppm ($-PCH_2-$) in the $^1H\{^{31}P\}$ NMR spectra are assigned to the PEt_3 groups in the inner and terminal [Pt] centers, respectively. The ratio between these two sets of signals provides another diagnostic for the length of the metal-terminated oligomers. In the $^{31}P\{^1H\}$ NMR spectra, there are two sets of peaks, at ~12.5 ppm (inner) with a pair of satellite peaks ($^1J_{P-Pt}$ = 2352−2370 Hz) and at ~16.2 ppm (terminal) with a pair of satellite peaks ($^1J_{P-Pt}$ = 2375−2390 Hz). These signals correspond to the PEt_3 groups on the inner and terminal [Pt] centers, respectively. The ratio between these two sets of peaks can also be used as an indicator for the length of the metal-terminated oligomers. The $^{13}C\{^1H\}$ NMR spectra of $\mathbf{L}_m\mathbf{[Pt]}_{m+1}Cl_2$ are separated into four groups: the signals between 147 and 120

(16) (a) Liu, Y.; Jiang, S. J.; Glusac, K.; Powell, D. H.; Anderson, D. F.; Schanze, K. S. *J. Am. Chem. Soc.* **2002**, *124*, 12412. (b) Onitsuka, K.; Harada, Y.; Takei, F.; Takahashi, S. *Chem. Commun.* **1998**, 643. (c) Yam, V. W.-W. *Acc. Chem. Res.* **2002**, *35*, 555.

Scheme 2

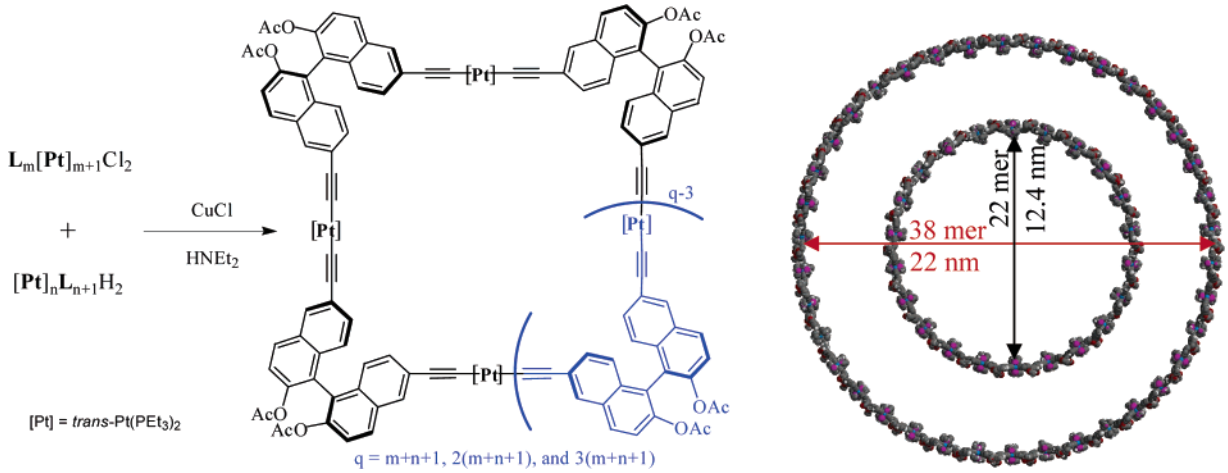

Table 1. Product Distributions and Yields for Metallocycles

reagents	products (yield %)[a] $(m+n+1)^b$	$2(m+n+1)^c$	$3(m+n+1)^d$	total yield (%)
$m = 1, n = 1$	**3** (37)	**6** (36)	**9** (11)	84
$m = 1, n = 2$	**4** (81)	**8** (13)	**12** (3)	97
$m = 3, n = 1$	**5** (73)	**10** (7)		80
$m = 3, n = 2$	**6** (85)	**12** (7)		92
$m = 3, n = 3$	**7** (75)	**14** (8)		83
$m = 5, n = 4$	**10** (69)			69
$m = 5, n = 5$	**11** (60)			60
$m = 5, n = 6$	**12** (65)			60
$m = 7, n = 6$	**14** (61)			61
$m = 11, n = 10$	**22** (38)			38
$m = 19, n = 18$	**38** (25)			25
$m = 31, n = 30$	N/A			

[a] Isolated yield after silica gel chromatography. [b] [1+1] cyclization products. [c] [2+2] cyclization products. [d] [3+3] cyclization products.

ppm are assigned to the naphthyl groups, the signals at ∼109 ppm and the signals between 102 and 82 ppm are assigned to the alkyne groups connected to the inner and terminal [Pt] centers, respectively, the signals at ∼16.4 (methylene) and ∼8.3 ppm (methyl) are assigned to the PEt_3 groups connecting to the inner [Pt] centers, while the signals at ∼14.6 (methylene) and ∼7.9 ppm (methyl) are assigned to the PEt_3 groups connecting to the terminal [Pt] centers, and the signals at ∼169 and 20.6 ppm are assigned to the acetyl groups.

Ligand-Terminated Open Oligomers $[Pt]_nL_{n+1}H_2$. The $^1H\{^{31}P\}$ NMR spectra of $[Pt]_nL_{n+1}H_2$ are well separated into four groups: the signals between 8.1 and 6.9 ppm assignable to the naphthyl groups, a singlet at ∼3.1 ppm assignable to terminal acetylenic proton, the signals at ∼2.19 and ∼1.22 ppm assignable to the PEt_3 groups, and the signals between 1.9 and 1.8 ppm assignable to the acetyl groups (Figure 2). In the $^1H\{^{31}P\}$ NMR spectra, the ligand **L** units display two major sets of peaks due to their two different chemical environments. For oligomer **[Pt](L**-H)$_2$, there is only one set of peaks in the ^1H NMR spectrum for the two terminal ligands. For longer oligomers $[Pt]_nL_{n+1}H_2$ ($n > 1$), a new set of peaks from the inner ligands appears at higher field. The stacked NMR spectra clearly show that the ratio between these two sets of peaks (inner:terminal) increases as the length of the ligand-terminated oligomer increases, consistent with the decrease of the percentage of the terminal ligand in the oligomers. In the $^{31}P\{^1H\}$ NMR spectra, there is only one set of peaks at ∼12.5 ppm with a pair of satellite peaks ($^1J_{P-Pt}$ = 2360−2370 Hz) corresponding to the PEt_3 groups on the inner [Pt] centers. The $^{13}C\{^1H\}$ NMR spectra of $[Pt]_nL_{n+1}H_2$ are separated into four groups: the signals between 148 and 118 ppm are assigned to the naphthyl groups, the signals at ∼109 ppm are assigned to the alkyne groups connected to the inner [Pt] centers, while two singlets at ∼83.5 and ∼77.8 ppm are assigned to the terminal alkyne groups, the signals at ∼16.3 (methylene) and ∼8.2 ppm (methyl) are assigned to the PEt_3 groups, and the signals at ∼169 and 21−20 ppm are assigned to the acetyl groups. The length of the ligand-terminated oligomers can also be estimated on the basis of the ratios between the above signals.

Metallocycles. In contrast to their open oligomeric starting materials, the $^1H\{^{31}P\}$, $^{31}P\{^1H\}$, and $^{13}C\{^1H\}$ NMR spectra of these chiral molecular polygons exhibit a single ligand environment, suggesting the formation of cyclic species of D_n symmetry (Figure 3). We have previously reported the single-crystal X-ray structure of the molecular square [*trans*-$(PEt_3)_2$Pt**L**]$_4$, which was prepared via a different route.[13b] Other spectroscopic data are also consistent with the formation of chiral molecular polygons (see below).

3.4. MALDI-TOF MS Characterization. The MALDI-TOF MS data show molecular ion peaks (M^+, $[M + Na]^+$, or $[M + K]^+$) and $[M - nPEt_3]^+$ peaks for open oligomers (up to m = 19 and n = 18) and chiral molecular polygons (up to 22mer). 2,5-Dihydroxybenzoic acid was used as the matrix for shorter open oligomers (m = 1, 2, 3, 5, 7 and n =1, 2, 3, 4, 5, 6) and smaller metallocycles (3mer to 8mer), while 1,8,9-trihydroxyanthracene was used as the matrix for longer open oligomers (m = 11, 19 and n = 10, 18) and larger metallocycles (9mer to 22mer). Detailed peak listings and their assignments can be found in the Supporting Information. The NMR spectroscopic and MALDI-TOF MS data thus confirmed the formation of open oligomers and metallocycles.

3.5. FT-IR, UV−Vis, and CD Spectroscopic Characterization. The IR spectrum of **L**-H_2 displays a strong absorption peak at ∼3300 cm^{-1} due to the terminal C≡C−H stretches. Upon the formation of ligand-terminated oligomers $[Pt]_nL_{n+1}H_2$, the peak at ∼3300 cm^{-1} become very weak, and a strong peak at ∼2090 cm^{-1} appears due to the C≡C stretches. As expected, the terminal C≡C−H stretches of **L**-H_2 at ∼3300 cm^{-1} disappear upon the formation of metal-terminated oligomers L_m-

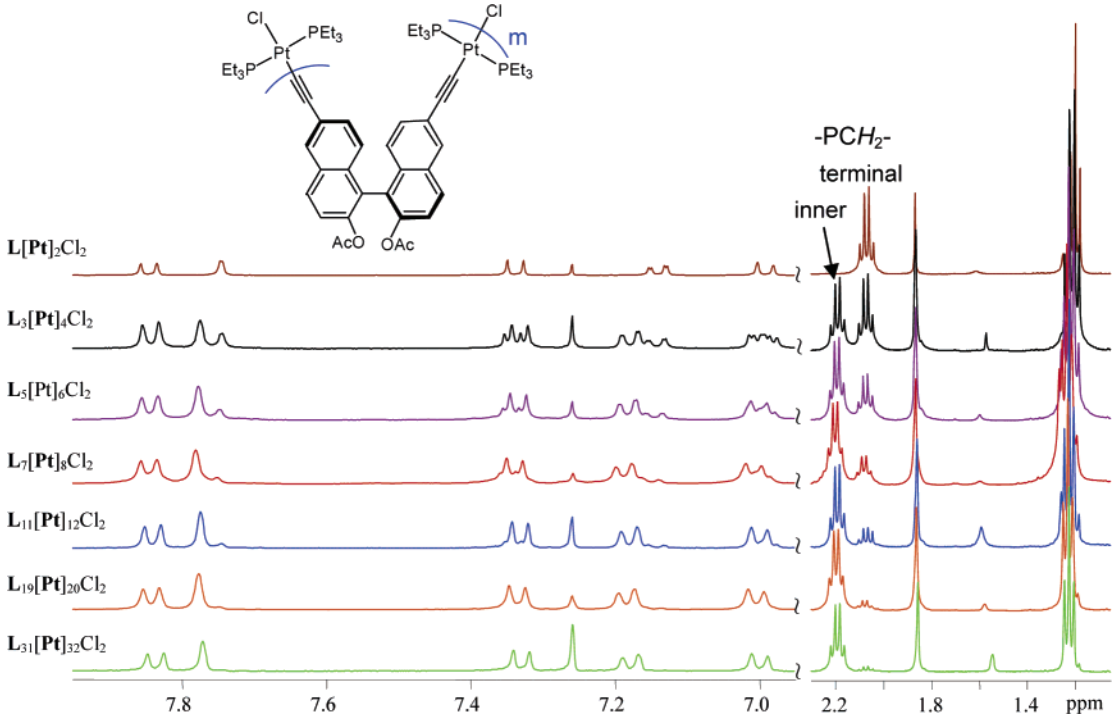

Figure 1. $^1H\{^{31}P\}$ NMR spectra of metal-terminated oligomers $\mathbf{L}_m[\mathbf{Pt}]_{m+1}Cl_2$.

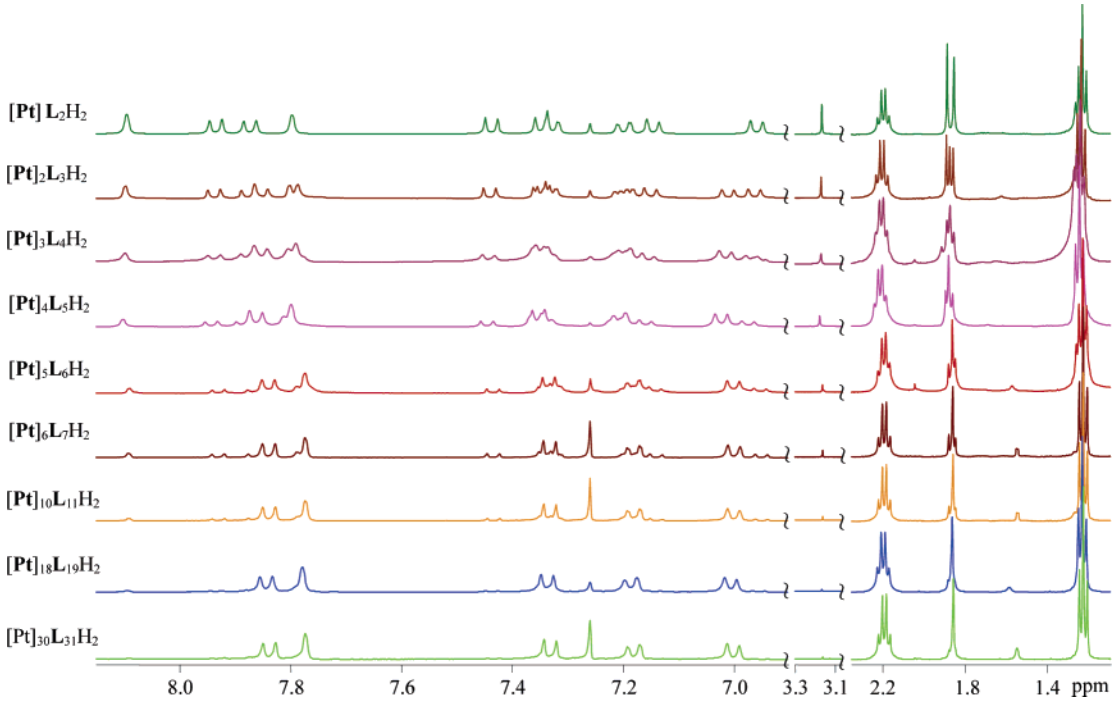

Figure 2. $^1H\{^{31}P\}$ NMR spectra of ligand-terminated oligomers $[\mathbf{Pt}]_n\mathbf{L}_{n+1}H_2$.

$[\mathbf{Pt}]_{m+1}Cl_2$ and metallocycles, and a strong peak at ~2090 cm^{-1} appears due to the C≡C stretches.

The UV−vis and CD experiments on metallocycles from 9mer to 38mer were carried out in CH_2Cl_2 due to the poor solubility of these metallocycles in acetonitrile. Smaller metallocycles, 3mer to 8mer, were dissolved in acetonitrile with varying amounts of dichloromethane. Since the cutoff of CH_2Cl_2 is 220 nm, the UV−vis and CD spectra of 9mer to 38mer in the region of 190−220 nm show no meaningful signals.

The electronic spectra of $\mathbf{L}$-H_2 show two major naphthyl $\pi\rightarrow\pi^*$ transitions at 236 and 250 nm and three weak, delocalized acetylenic $\pi\rightarrow\pi^*$ transitions at 280, 288, and 310 nm. Upon the formation of open oligomers and metallocycles, a new intense peak at ~226 nm appears, assignable to the *trans*-Pt-$(PEt_3)_2$ moiety (Figure 4). The acetylenic $\pi\rightarrow\pi^*$ transitions red-shift and split into two intense broad peaks at ~340 and ~360 nm, a result of mixing of Pt p-orbitals into the acetylenic $\pi\rightarrow\pi^*$ bands. The two major peaks at ~274 and 295 nm are assigned to the naphthyl $\pi\rightarrow\pi^*$ transitions. The extinction coefficients increase as the length of the open oligomers and the size of the metallocycles increase, consistent with the presence of an increasing number of *trans*-Pt$(PEt_3)_2$ and $\mathbf{L}$ building units.

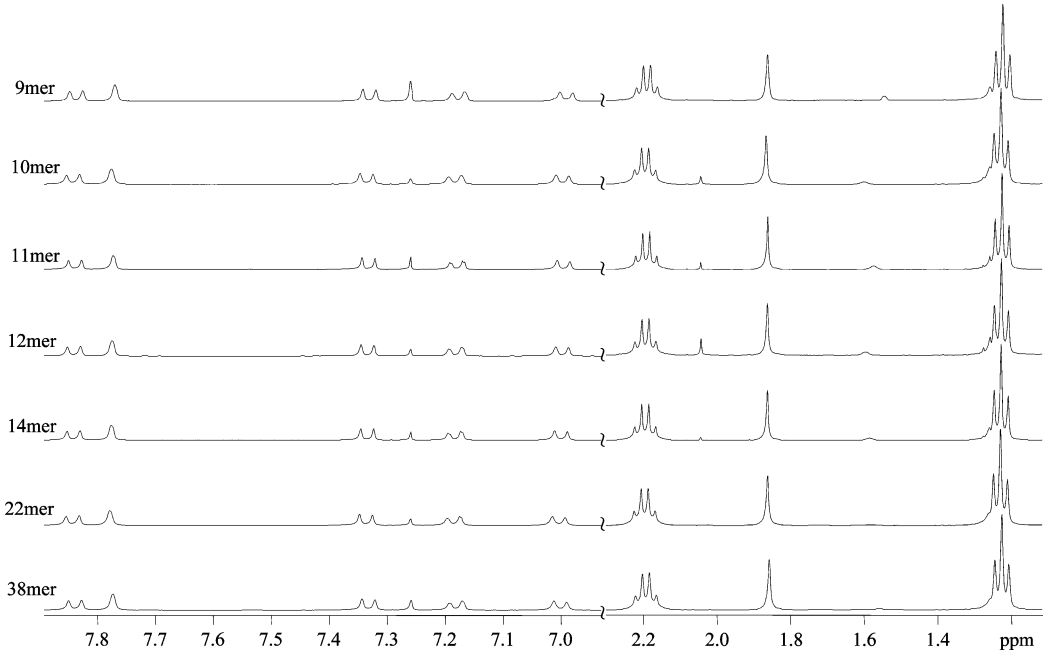

Figure 3. $^{1}H\{^{31}P\}$ NMR spectra of metallocycles [*trans*-$(PEt_3)_2Pt\mathbf{L}]_q$ ($q = 9-38$).

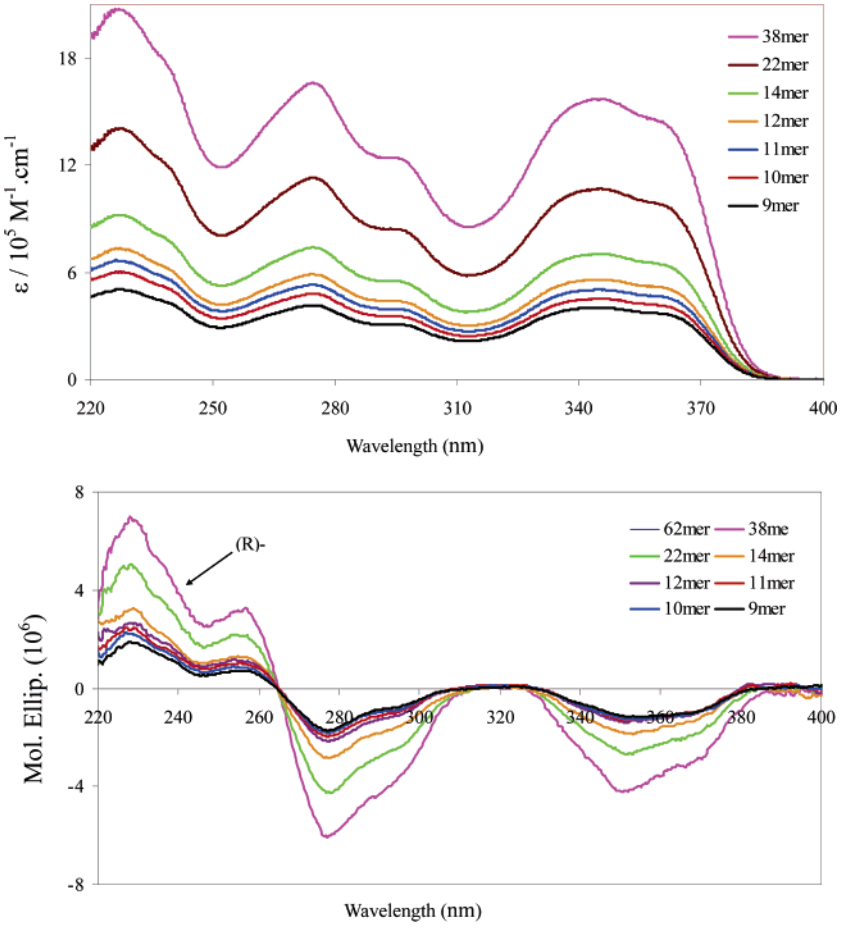

Figure 4. UV−vis (top) and CD (bottom) spectra of metallocycles (*R*)-[*trans*-$(PEt_3)_2Pt\mathbf{L}]_q$ ($q = 9-38$) in CH_2Cl_2.

The CD spectrum of **L**-H_2 exhibits two major bisignate bands for the naphthyl $\pi\rightarrow\pi^*$ transitions at ~236 and ~250 nm and one minor band at ~290 nm for the acetylenic $\pi\rightarrow\pi^*$ transition. Upon formation of open oligomers and metallocycles, the bisignate naphthyl $\pi\rightarrow\pi^*$ bands red-shift to ~254 and 278 nm, whereas the acetylenic $\pi\rightarrow\pi^*$ CD signal appears as two bands at ~350 and ~370 nm. A new intense band also appears at ~225 nm due to the chiral arrangement of the PEt_3 groups on the Pt center in the chiral environment of the bridging ligands. The CD signals increase steadily as the size of the metallocycle

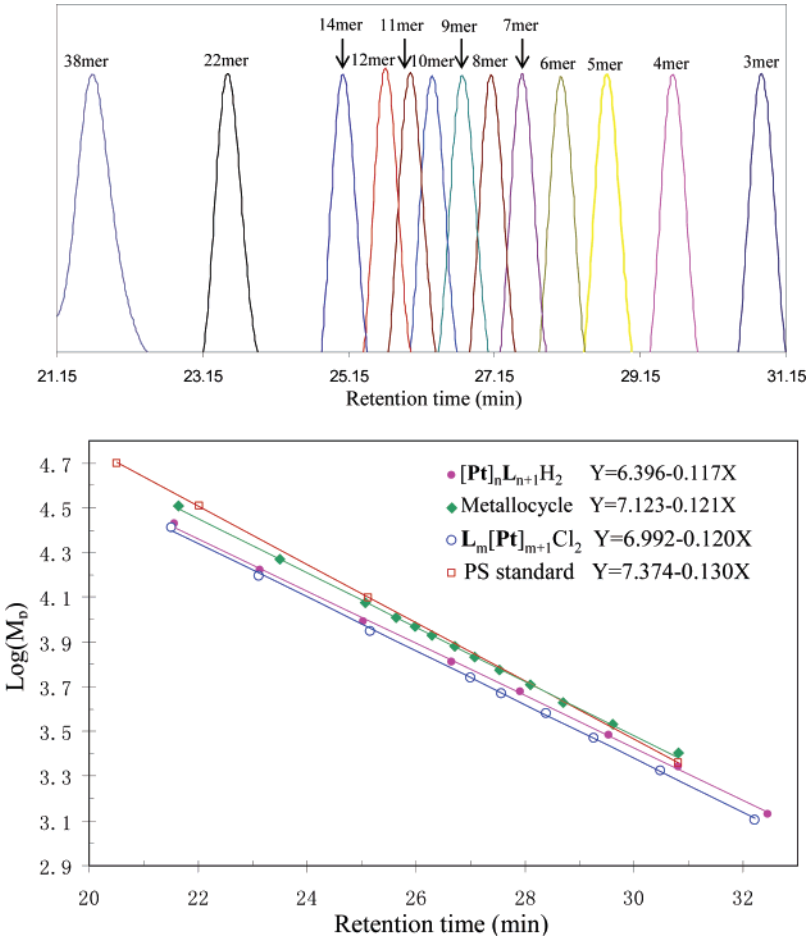

Figure 5. Retention times of the metallocycles in SEC (top) and plot of log(M_p) vs retention time for $\mathbf{L}_m[\mathbf{Pt}]_{m+1}Cl_2$, $[\mathbf{Pt}]_n\mathbf{L}_{n+1}H_2$, $[trans\text{-}(PEt_3)_2Pt\mathbf{L}]_q$, and polystyrene standards (bottom).

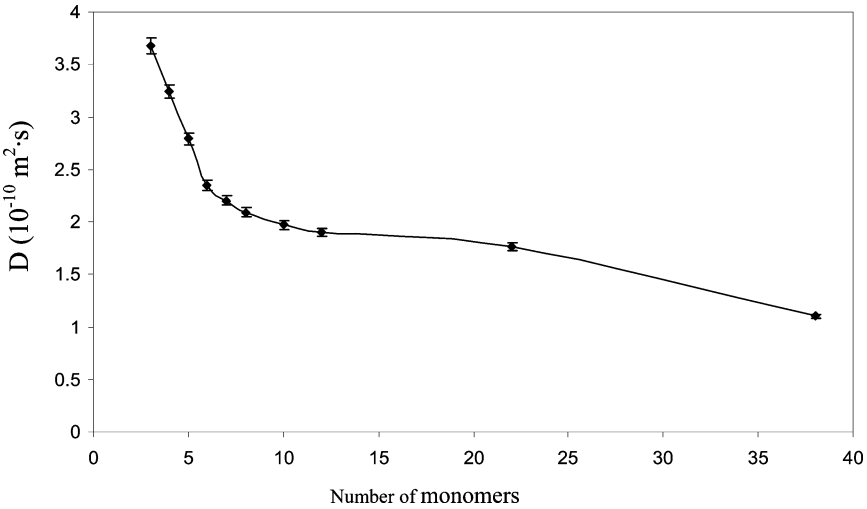

Figure 6. Dependence of D coefficients on the number of monomers for the metallocycles.

increases, consistent with an increasing number of *trans*-Pt-$(PEt_3)_2$ and **L** building units (Figure 4).

3.6. Size Exclusion Behaviors of Open Oligomers and Metallocycles. The mesoscopic nature of molecular polygons presents a significant challenge for their characterization. Although the identity of metal- and ligand-terminated oligomers has been unambiguously established on the basis of NMR data, MALDI-TOF MS, and microanalysis results, the differentiation of sizes among the molecular polygons is based exclusively on MALDI-TOF MS data. We have resorted to SEC to estimate the sizes of open oligomers and metallocycles as well as to prove the purity of the metallocycle products. As shown in Figure 5, each metallocycle shows a very narrow band in its SEC chromatograph. The plots of log(M_p) vs retention time can be linearly fitted for open oligomers and metallocycles. The metallocycles fall essentially on a line that matches well with that of polystyrene (PS) standards, thus confirming their formulation. The line of the metallocycles has a slightly larger

Scheme 3

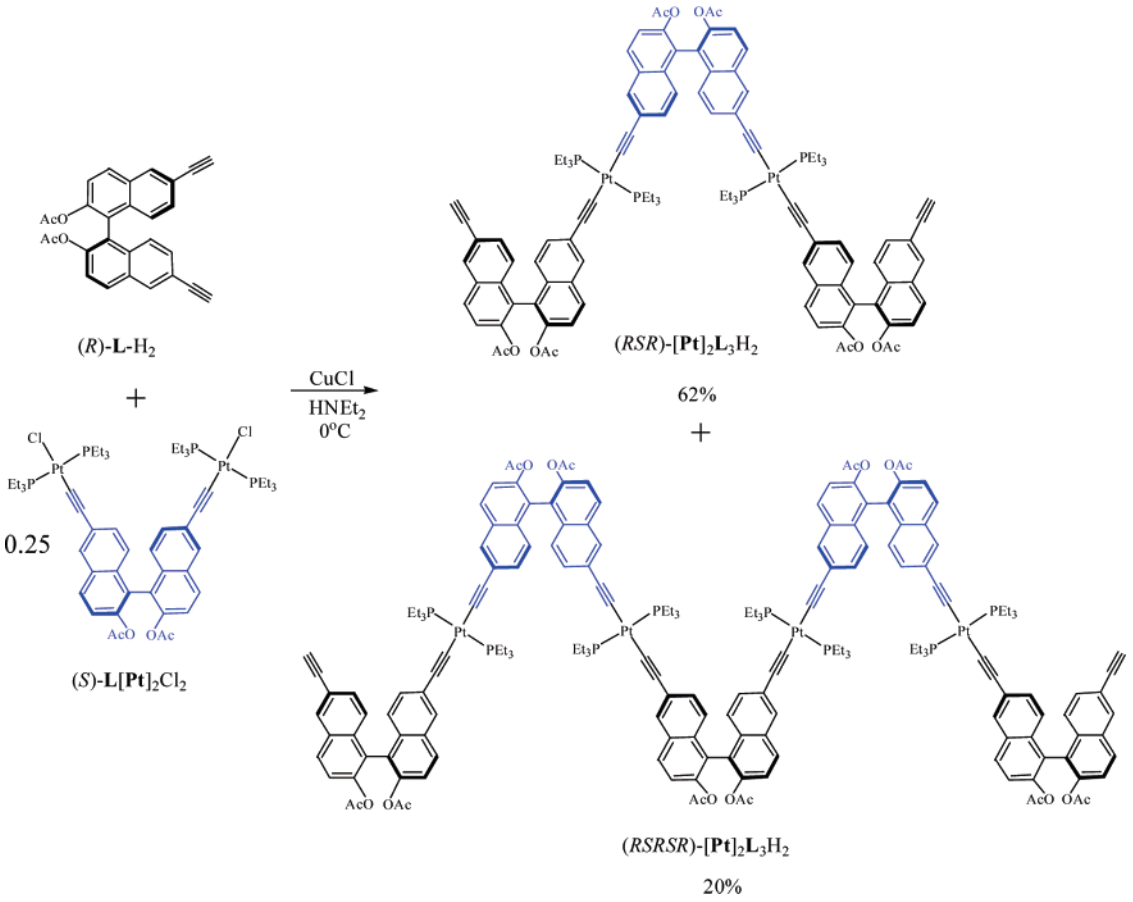

slope (−0.121) than that of PS standards (−0.130). A larger slope indicates more drastic dependence of retention time on log(M_p) and thus suggests a more rigid structure. The metal- and ligand-terminated oligomers, on the other hand, fell on a different line (with even larger slopes) than the PS standards.

3.7. Diffusion-Ordered NMR Spectroscopic Study of Metallocycles. Diffusion-ordered NMR spectroscopy (DOSY) is a powerful technique for assessing dynamic radii of molecules on the basis of their diffusion characteristics.[17] We carried out DOSY studies of the metallocycles (from 3mer to 38mer) on a Varian INOVA 600 NMR spectrometer equipped with a 20 A gradient driver. The metallocycles were dissolved in $CDCl_3$ with a concentration of 8.3 mg/mL. Acquisition parameters were optimized using a standard 1D ^1H experiment and the BPPSTE or BPPLED pulse sequence with the minimum gradient level.[15]

Figure 6 is a plot of the *D* coefficients vs the number of monomers present in the metallocycles. The *D* coefficient of the singlet at ~7.73 ppm due to the resonance of proton H5 in the naphthalene was used in Figure 6. For each sample, the *D* coefficient value is obtained from more than three measurements. It is clear from Figure 6 that the *D* coefficients decrease as the size of cycles increases, which is consistent with the SEC results.

3.8. Synthesis of *Non-homochiral* Molecular Squares. The stepwise assembly of molecular polygons provides a facile route to precisely control the structure of the metallocycles. Different sizes and shapes of metallocycles have been prepared successfully, as illustrated above. All the metallocycles described earlier, consisting of enantiopure bridging ligands, were of the same absolute configuration (homochiral). We have also introduced ligands with the opposite configuration to generate *non-homochiral* metallocycles via the stepwise assembly method.

The oligomers (*RSR*)-[**Pt**]$_2$**L**$_3$H$_2$ and (*RSRSR*)-[**Pt**]$_4$**L**$_5$H$_2$ were prepared by treating (*R*)-**L**-H$_2$ with 0.25 equiv of (*S*)-**L**[**Pt**]$_2$Cl$_2$ at 0 °C in deaerated CH_2Cl_2 and NEt_3 in the presence of CuCl catalyst (Scheme 3). Molecular square (*RSRS*)-[*trans*-(PEt$_3$)$_2$-Pt**L**]$_4$ and octagon (*RSRSRSRS*)-[*trans*-(PEt$_3$)$_2$Pt**L**]$_8$ were obtained in high yields (76% and 8%, respectively) by treating (*RSR*)-[**Pt**]$_2$**L**$_3$H$_2$ with 1 equiv of (*S*)-**L**[**Pt**]$_2$Cl$_2$ at room temperature in deareated CH_2Cl_2 and NEt_3 in the presence of a catalytic amount of CuCl. Molecular square (*RRRS*)-[*trans*-(PEt$_3$)$_2$Pt**L**]$_4$ and octagon (*RRRSRRRS*)-[*trans*-(PEt$_3$)$_2$Pt**L**]$_8$ were prepared in 83% and 10% yield, respectively, by treating (*RRR*)-[**Pt**]$_2$**L**$_3$H$_2$ with 1 equiv of (*S*)-**L**[**Pt**]$_2$Cl$_2$ at room temperature in deareated CH_2Cl_2 and NEt_3 in the presence of a catalytic amount of CuCl. Molecular square (*RRSS*)-[*trans*-(PEt$_3$)$_2$Pt**L**]$_4$ and octagon (*RRSSRRSS*)-[*trans*-(PEt$_3$)$_2$Pt**L**]$_8$ were prepared in 76% and 12% yield, respectively, by treating (*RR*)-**L**$_2$[**Pt**]$_3$Cl$_2$ with 1 equiv of (*SS*)-[**Pt**]**L**$_2$H$_2$ at room temperature in deareated CH_2Cl_2 and NEt_3 in the presence of a catalytic amount of CuCl. *The present synthetic approach thus allows the synthesis of all the four diastereomeric molecular squares by simply starting from building blocks of desired chirality.*

The non-homochiral molecular squares and octagons were characterized by $^1H\{^{31}P\}$, $^1P\{^1H\}$, and $^{13}C\{^1H\}$ NMR spec-

(17) (a) Avram, L.; Cohen, Y. *J. Am. Chem. Soc.* **2002**, *124*, 15148. (b) Stahl, N. G.; Zuccaccia, C.; Jensen, T. R.; Marks, T. J. *J. Am. Chem. Soc.* **2003**, *125*, 5256. (c) Morris, K. F.; Johnson, C. S. *J. Am. Chem. Soc.* **1993**, *115*, 4291.

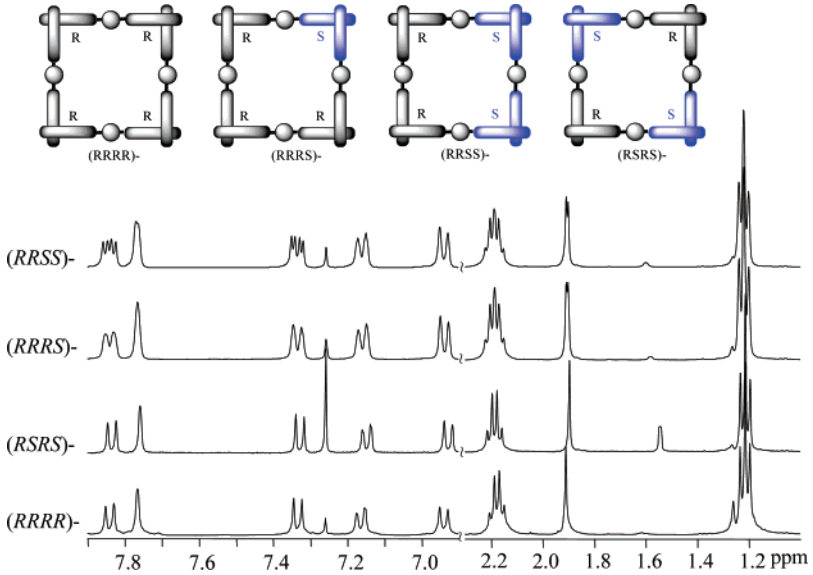

Figure 7. $^1H\{^{31}P\}$ NMR spectra of non-homochiral and homochiral squares [*trans*-$(PEt_3)_2Pt$**L**$]_4$.

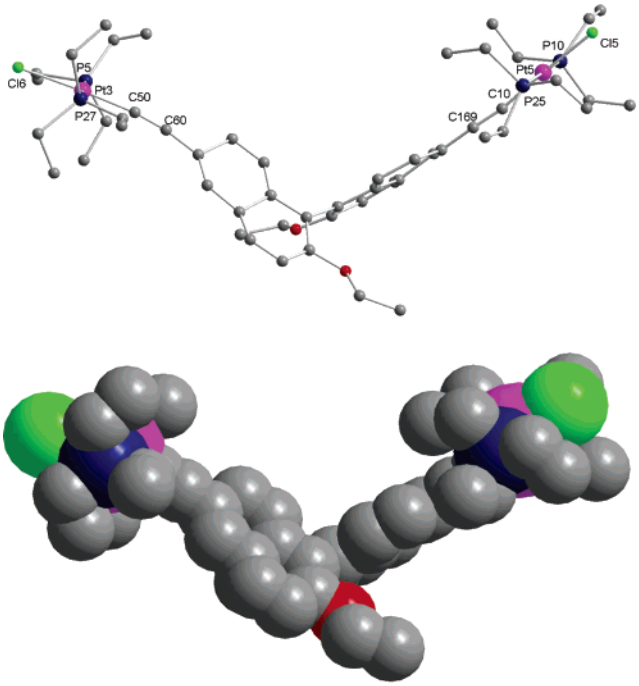

Figure 8. Single-crystal X-ray structure (top) and a space-filling model (bottom) of (**L**-OEt)[**Pt**]$_2Cl_2$.

troscopy and MALDI-TOF MS. The $^1H\{^{31}P\}$, $^1P\{^1H\}$, and $^{13}C\{^1H\}$ NMR spectra of molecular square (*RSRS*)-[*trans*-$(PEt_3)_2Pt$**L**$]_4$ and octagon (*RSRSRSRS*)-[*trans*-$(PEt_3)_2Pt$**L**$]_8$ show a single ligand environment due to the same chemical environments of both (*R*)- and (*S*)-bridging ligands, which is consistent with D_{2d} symmetry of the square and D_{4d} symmetry of the octagon. In contrast, the $^1H\{^{31}P\}$ and $^1P\{^1H\}$ NMR spectra of the molecular square (*RRSS*)-[*trans*-$(PEt_3)_2Pt$**L**$]_4$ and octagon (*RRSSRRRS*)-[*trans*-$(PEt_3)_2Pt$**L**$]_8$ show two sets of peaks, corresponding to two different chemical environments for the naphthyl groups and [**Pt**] centers (Figure 7), corresponding to C_{2h} symmetry of the square and D_{2d} symmetry of the octagon. The $^1H\{^{31}P\}$ NMR spectra of the molecular square (*RRRS*)-[*trans*-$(PEt_3)_2Pt$**L**$]_4$ and octagon (*RRRSRRRS*)-[*trans*-$(PEt_3)_2Pt$**L**$]_8$ show broad peaks due to the overlap of signals from the naphthyl groups in four different chemical environments, while their $^1P\{^1H\}$ NMR spectra show two set of peaks from the PEt_3 groups in two different environments, corresponding to C_2 symmetry of the square and D_2 symmetry of the octagon.

The MALDI-TOF MS data show ionized peaks of $[M + H]^+$, $[M + Na]^+$, and $[M + K]^+$, consistent with the formation of cyclic species. The retention times of the non-homochiral squares and octagons are a little larger than those of the corresponding homochiral squares and octagons, which indicate smaller sizes of non-homochiral cycles. This is because the non-homochiral cycles adopt butterfly structures rather than the more planar geometry seen in the homochiral metallocycles. This has been supported by the single X-ray structures of the ethyl-protected squares, which are discussed in the next section.

3.9. Ethyl-Protected Metallocycles. The chiral bridging ligand 2,2′-diethoxy-6,6′-diethynyl-1,1′-binaphthalene (**L**-OEt-H_2) was also used to construct molecular polygons with *trans*-$Pt(PEt_3)_2$ metal connectors. By using the methods adopted for the **L**-based oligomers and metallocycles, **L**-OEt-based oligomers (**L**-OEt)[**Pt**]$_2Cl_2$, [**Pt**](**L**-OEt)$_2H_2$, [**Pt**]$_2$(**L**-OEt)$_3H_2$, and homochiral metallocycles [*trans*-$(PEt_3)_2Pt$(**L**-OEt)$]_q$ ($q = 3$ and 4) were prepared. The homochiral molecular triangle [*trans*-$(PEt_3)_2Pt$(**L**-OEt)$]_3$ was prepared by treating (**L**-OEt)[**Pt**]$_2Cl_2$ with 1 equiv of [**Pt**](**L**-OEt)$_2H_2$ in deareated CH_2Cl_2 and $HNEt_2$ in the presence of a catalytic amount of CuCl, while the homochiral molecular square [*trans*-$(PEt_3)_2Pt$(**L**-OEt)$]_4$ was prepared by treating (**L**-OEt)[**Pt**]$_2Cl_2$ with 1 equiv of **L**-OEt-H_2 in deareated $HNEt_2$ in the presence of a catalytic amount of CuCl. The *meso*-metallocycle (*RSRS*)-[*trans*-$(PEt_3)_2Pt$(**L**-OEt)$]_4$ was synthesized by treating (*S*)-(**L**-OEt)[**Pt**]$_2Cl_2$ with 1 equiv of (*R*)-**L**-OEt-H_2 in deareated $HNEt_2$ in the presence of a catalytic amount of CuCl.

The molecular triangles and squares were characterized by $^1H\{^{31}P\}$ and $^{31}P\{^1H\}$ NMR spectroscopy and MALDI-TOF MS. The *meso*-square (*RSRS*)-[*trans*-$(PEt_3)_2Pt$(**L**-OEt)$]_4$ was also characterized by single-crystal X-ray crystallography.

A single-crystal X-ray diffraction study on (**L**-OEt)[**Pt**]$_2Cl_2$ unambiguously demonstrated the formation of metal-terminated oligomer (Figure 8). (**L**-OEt)[**Pt**]$_2Cl_2$ crystallized in the chiral orthorhombic space group $P2_12_12_1$. Two *trans*-$Pt(PEt_3)_2Cl$

Scheme 4

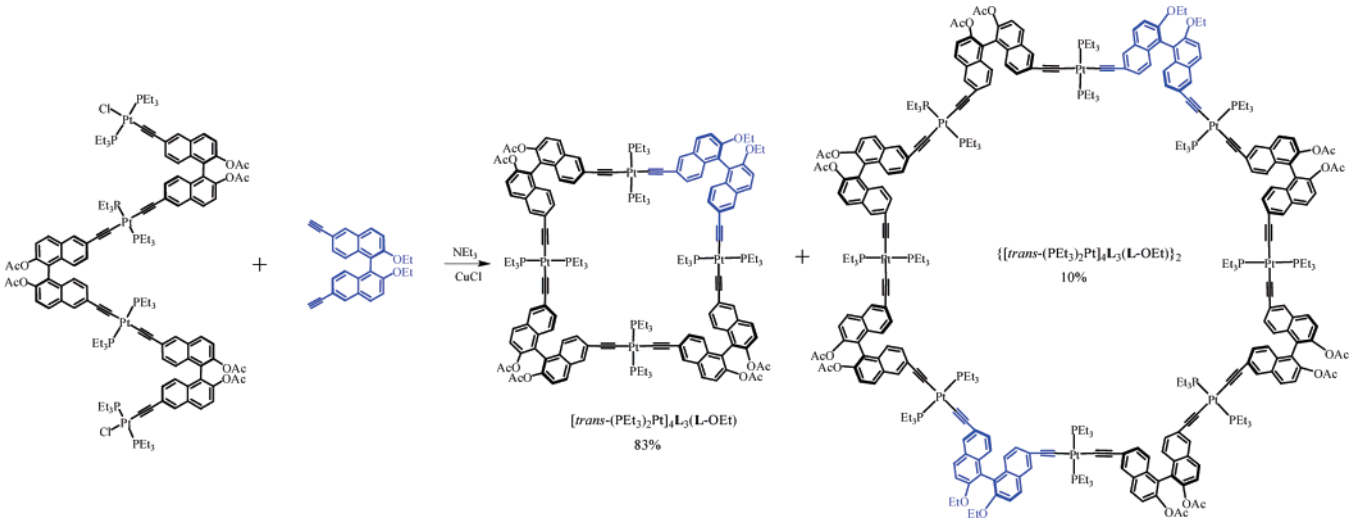

groups are connected to the two ends of the ligand **L**-OEt unit. The asymmetric unit of the crystal contains four molecules of (**L**-OEt)[**Pt**]$_2$Cl$_2$, with the dihedral angles between the two naphthalene rings being 109.7, 107.9, 101.1, and 100.9°, respectively.

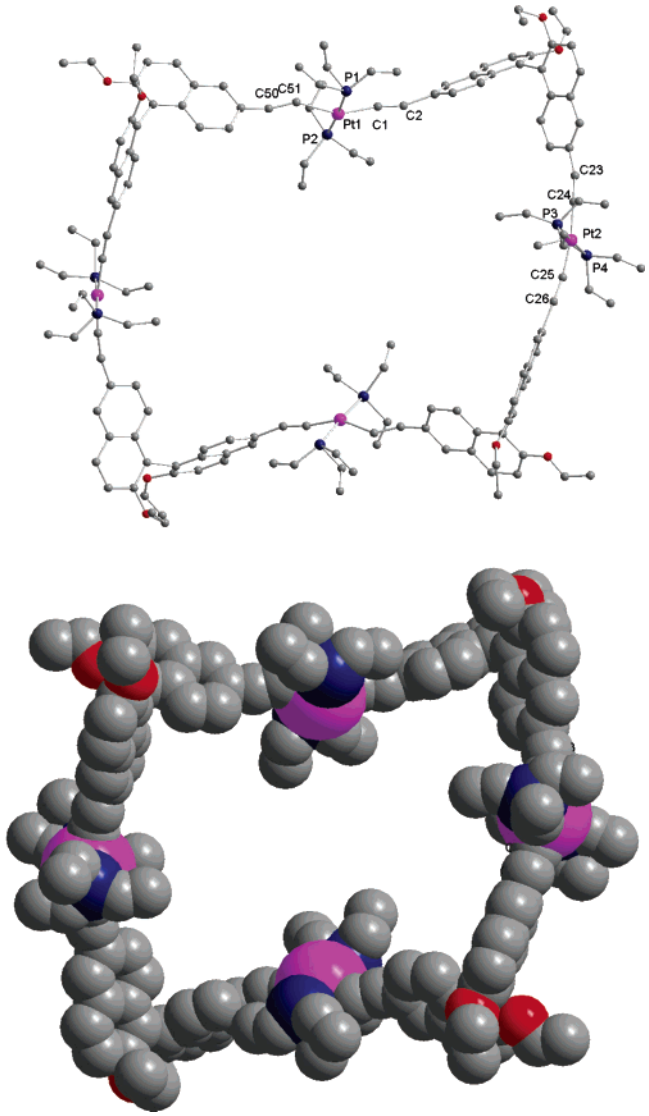

Figure 9. Single-crystal X-ray structure (top) and a space-filling model (bottom) of (*RSRS*)-[*trans*-(PEt$_3$)$_2$Pt(**L**-OEt)]$_4$.

A single-crystal X-ray diffraction study on (*RSRS*)-[*trans*-(PEt$_3$)$_2$Pt(**L**-OEt)]$_4$ confirmed the formation of a *meso*-metallocycle. Compound (*RSRS*)-[*trans*-(PEt$_3$)$_2$Pt(**L**-OEt)]$_4$ crystallizes in the chiral monoclinic space group *C*2 with a very twisted (butterfly) structure. A 2-fold axis of crystallographic symmetry is present in the molecules of (*RSRS*)-[*trans*-(PEt$_3$)$_2$Pt(**L**-OEt)]$_4$ in the solid state. The dihedral angles between the two naphthalene rings are 78.9 and 69.4°. The Pt centers adopt distorted square planar geometries (Figure 9).

3.10. Introduction of Symmetry Probes in the Metallocycles. We have also introduced symmetry probes into chiral metallocycles by using bridging ligands with different protecting groups. Homochiral molecular square *trans*-[(PEt$_3$)$_2$Pt]$_4$**L**$_3$(**L**-OEt) and octagon {*trans*-[(PEt$_3$)$_2$Pt]$_3$**L**$_3$(**L**-OEt)}$_2$ were prepared by treating **L**$_3$[**Pt**]$_4$Cl$_2$ with 1 equiv of **L**-OEt-H$_2$ in the presence of a catalytic amount of CuCl in deareated CH$_2$Cl$_2$ and NEt$_3$ at room temperature (Scheme 4). The molecular square and octagon resulted from [1+1] and [2+2] cyclization processes, respectively, and possess two types of ligands with the ratio of **L**:**L**-OEt = 3:1. The two ligands **L**-OEt are separated by three ligands **L** in the octagon, which results in D_2 symmetry. The molecular square and octagon were characterized by ^{1}H{^{31}P} and ^{31}P{^{1}H} NMR spectroscopy and MALDI-TOF MS, and the square was characterized by ^{13}C{^{1}H} NMR spectroscopy as well.

The ^{1}H{^{31}P}, ^{13}C{^{1}H}, and ^{31}P{^{1}H} NMR spectra of these polygons show two sets of peaks resulting from the introduction of ligand **L**-OEt (Figure 10). The ^{1}H{^{31}P} NMR spectra of the square and octagon show signals from ligands **L** and **L**-OEt in a ratio of 3:1. The singlet at 7.76 ppm is assigned to the H5 in ligand **L**, while the singlet at 7.71 ppm is assigned to H5 in ligand **L**-OEt. The signals at 4.0 and 1.05 ppm are assigned to the ethyl groups in **L**-OEt. The singlet at 1.87 ppm is assigned to the acetyl groups in **L**. Similar characteristic peaks are also observed in the ^{1}H{^{31}P} NMR spectrum of the octagon. The ^{31}P{^{1}H} NMR spectra of the molecular square and octagon show two singlets with the ratio of 1:1, assignable to the **L**-Pt(PEt$_3$)$_2$-(**L**-OEt) groups and **L**-Pt(PEt$_3$)$_2$-**L**, respectively. As expected,

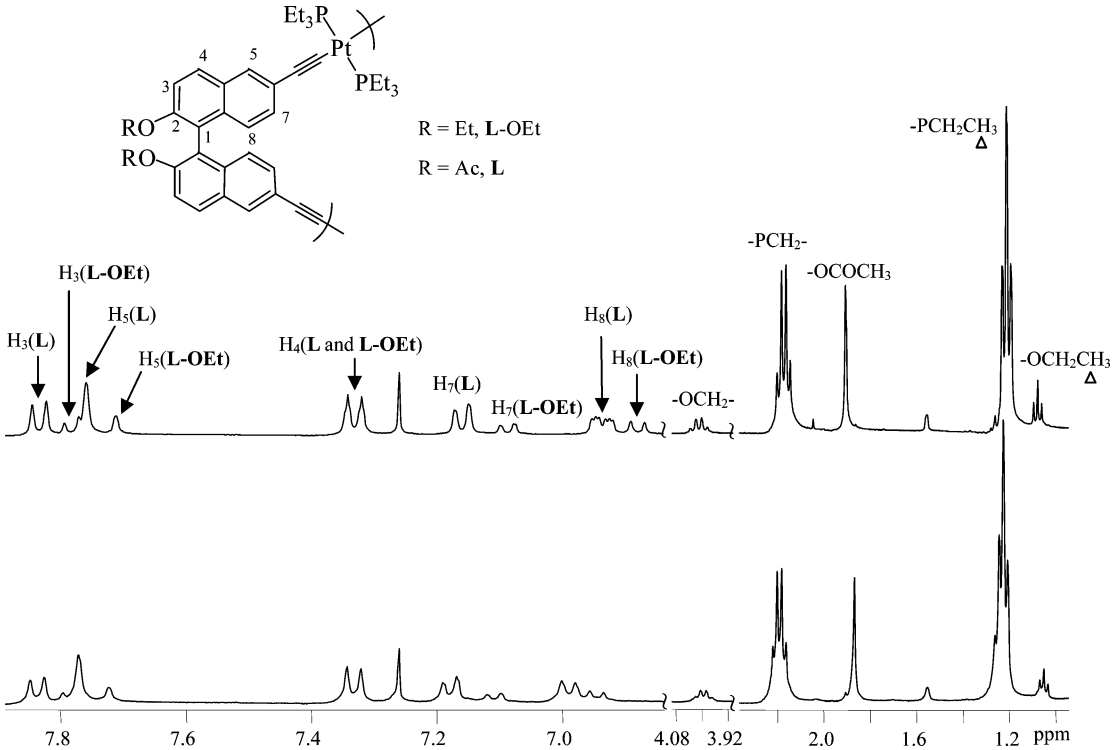

Figure 10. $^{1}H\{^{31}P\}$ NMR spectra of $\{trans\text{-}[(PEt_3)_2Pt]_3\mathbf{L}_3(\mathbf{L}\text{-OEt})\}_n$ ($n = 1$, top; $n = 2$, bottom).

the $^{13}C\{^{1}H\}$ NMR spectrum of the molecular square shows signals from both ligands **L** and **L**-OEt.

We have previously shown that the acetyl protecting groups in the metallocycles can be readily removed by treating [*trans*-$(PEt_3)_2Pt\mathbf{L}]_n$ with inorganic bases to give hydroxyl-containing metallocycles.[13b] For example, the molecular square [*trans*-$(PEt_3)_2Pt\mathbf{L}]_4$ was treated with K_2CO_3 in MeOH and THF to afford metallocycle [*trans*-$(PEt_3)_2Pt(\mathbf{L}\text{-OH})]_4$ with hydroxy functional groups. We have shown that such hydroxyl-containing metallocycles can be converted to new metallocycles with other functionalities, such as octadecyl chains or Frechét dendrons.

4. Discussion

As described above, we have carried out three key experiments to provide further proof that the homochiral metallocycles described in section 3.2 come from [1+1], [2+2], and [3+3] cyclization processes. First, both homochiral and *meso*-metallocycles with ethyl protecting groups can be similarly prepared and thus establish the generality of the present synthetic methodologies. Second, we prepared 4mer and 8mer with acetyl and ethyl protecting groups in a 3:1 ratio in section 3.10. By introducing different protecting groups, we have now added a symmetry probe which allows the unambiguous assignments of 4mer and 8mer on the basis of the NMR integrations and MALDI-TOF MS. Third, we have also prepared non-homochiral metallocycles by using ligands of opposite chirality. The *meso*-tetramer with the ethyl protecting groups has been characterized by X-ray crystallography. Most importantly, the isolation of metallocycles containing both ethyl and acetyl groups and non-homochiral metallocycles gives further proof that these metallocycles come from [1+1], [2+2], and [3+3] cyclization processes.

The well-fitted linear plot of SEC data and the DOSY experimental data provide a way to estimate the sizes of these metallocycles, and also provide us information about their rigid and compact structures. The ready synthesis of homochiral and non-homochiral metallocycles with ethyl protecting groups further proved the effectiveness of this synthetic strategy. The ready removal of the acetyl group to give hydroxyl-containing cycles provides a platform to further functionalize these metallocycles with different functional groups. The symmetry probe method provides precise control over the structures of these metallocycles by using different bridging ligands in specific positions.

5. Summary

We have successfully synthesized and characterized nanoscopic and mesoscopic chiral molecular polygons, and their sizes were characterized by SEC chromatography and DOSY NMR spectroscopy. The present synthetic methodology was also extended to the synthesis of non-homochiral metallocycles of very different topologies and macrocyclic structures with additional functional groups precisely placed at different positions. Such metallocycles provide interesting building blocks for the construction of larger functional structures that cannot be accessed from a top-down approach.

Acknowledgment. We thank NSF (CHE-0512495) and ACS-PRF for financial support. W.L. is a Camille Dreyfus Teacher-Scholar. We are grateful to Dr. Marc ter Horst for his invaluable help with DOSY experiments and Dr. Chuan-De Wu for help with X-ray structure determinations.

Supporting Information Available: Detailed experimental procedures and spectroscopic data (PDF) and X-ray crystallographic data (CIF). This material is available free of charge via the Internet at http://pubs.acs.org.

JA0633013